JCAMECH

Vol. 48, No. 1, June 2017, pp 1-14
DOI: 10.22059/jcamech.2017.232261.139

Dielectrophoretic effect of nonuniform electric fields on the protoplast cell

Kia Dastani, Mahdi Moghimi Zand*, Amin Hadi

School of Mechanical Engineering, University of Tehran, Tehran, Iran

Received: 29 Apr. 2017, Accepted: 8 June. 2017

Abstract

In recent decades the effects of magnetic and electric fields on living cells and organisms have gained the increased attention of researchers. In recent years, dielectrophoresis based microfluidics systems have been used to manipulate biological micro particles, such as red blood cells, white blood cells, platelets, cancer cells, bacteria, yeast, microorganisms, proteins, DNA, etc. So most previous researchers have studied particle trajectory under the application of electric field in order to better design of such micro devices. In the current study the effect of nonuniform electric field on a single cell is investigated. A neutral particle polarizes in the presence of electric field. It causes local change in electrostatic potential distribution and local nonuniformity in electric field. These changes are ignored in previous researches and effective dipole moment (EDM) approximation is applied to predict the DEP force exerted on cells. In the present research the effect of cell on electrostatic potential distribution and electric stresses acting on cell surface is studied. To this end, the cell shape and internal boundary conditions on cell surface must be considered in computational domain. To do this, Immersed Interface Method (IIM) which is a modified finite difference method is employed. Some numerical results are presented to show the good accuracy of mentioned numerical method. The electric stresses on cell surface are calculated by Maxwell Stress Tensor (MST). Also some results are presented to validate the numerical solution and investigate the accuracy of EDM approximation. Other electrokinetic effects such as electrophoresis and electro-osmosis are neglected in this study.

Keywords: Dielectrophoresis, protoplast cell, Maxwell stress tensor, Immersed Interface Method

1. Introduction

Dielectrophoresis phenomena has been introduced by H. A. Pohl who performed experiments with applying a non-uniform AC and DC electric field on a suspension of small plastic particles and dielectric liquids [1]. He observed that particles move under the application of non-uniform electric field. The force applied on particles in the presence of non-uniform electric field is called dielectrophoresis (DEP) force. DEP force depends on dielectric properties of cell and buffer fluid. So the magnitude and direction of DEP force is different for different cell types. This is the basis of designing microsystems for the purpose of manipulating biological particles such as cell, DNA, gene, etc. which is greatly important in various biotechnological applications [2-5]. Several researches have been done recently to design microsystems to manipulate bioparticles using electrokinetic forces [6-8]. Some important advantages of microfluidics systems are low energy consumption, low cast and short time reaction [9].

* Corresponding Author. Tel.: +98-21-61114807; Fax: +98-21-88013029
Email Address: mahdimoghimi@ut.ac.ir

The dielectrophoresis phenomena can be explained by charge distribution on particle surface. It polarizes, when a neutral particle is exposed to an electric field. Thus positive and negative induced charges accumulate on inner and outer side of particle surface. If the applied electric field is uniform the resultant of Columbic forces applied on charges is zero, but if it is non-uniform the particle experiences a net DEP force which drives it toward higher or lower electric field. If the particle polarizes more than buffer fluid, the particle moves toward high electric field region. This phenomenon is called positive dielectrophoresis (pDEP). Otherwise the particle moves toward lower electric field which is called nDEP. The DEP force type depends on dielectric properties of particle and medium.

Particle trajectory is highly important in microfluidics systems designed for separating different particles. Microfluidics systems designed for separating, particle assembly, and filtration work based on force variation applied on different particle types [10]. For further studies on such microfluidic devices, study [35,36].

In the most of previous researches, effective dipole moment approximation has been considered to study the behavior of particle in the presence of electric field and investigating particle trajectory [11-13]. In some researches multipole approximation is used to calculate DEP force [14,15]. In another research, Kua et.al. have presented an analytical method, called Wiener-Hopf, to solve the electrostatic equation and calculate multipolar DEP forces [16]. They have investigated the particle trajectory caused by dipole, quadrupole and octapole forces in the presence of non-uniform electric field and concluded that considering the first order force is sufficient to determine the particle trajectory. Point dipole approximation is accurate when the particle size is not comparable to the device size. Otherwise local non-uniformities of the induced field due to the particles is not negligible and higher order multipolar terms must be retained [17]. Dipole moment has been calculated and presented in literature for several ideal-shaped geometries. In previous researches, higher-order forces have been calculated for spherical particles. While the shape of cells and biological particles is not spherical in reality and polar moments are heavily dependent on particle shape. In some researches, higher order DEP force is calculated for some simple non-spherical particles using multipolar approximation [18,19].

Effective dipole approximation (EDM) is easy to use but has the disadvantage of being very hard to apply when the particle shape is not spherical and less accuracy while the particle size is not negligible. In these cases, Maxwell stress tensor (MST) can be used to calculate DEP force [19,20]. For using this method, governing electrostatic or quasi-electrostatic equations must be solved in the presence of particle. In a research D. L. Hous and H. Luo have determined the trajectory of a non-conducting colloidal sphere in a bent pore [20]. They have calculated the DEP force using MST and EDM and compered the trajectory determined by each method. Y. Liu et al. have used immersed electrokinetic method to solve the quasi-electrostatic equation in the presence of particle with the aim of calculating Maxwell stress tensor [21].

The biological effects of magnetic field and electric field have captivated the interest of many researches in recent years. Many works have been done on the response of living organisms to low, moderate and strong magnetic and electric fields [22-27]. In a research a theoretical framework has been presented to understand the effect of high gradient magnetic field on intercellular processes and cell life [28]. One of the most important effects of electric field on cells is the dielectrophoresis phenomenon. In most previous researches the dielectrophoretic effect of electric field on a cell group has been studied [29-30]. But in the present work we have studied the interaction of electric field and a single cell. To the best of the researchers' knowledge, in the literature, there is no study carried out into studying the effect of cells on electrostatic potential distribution which leads to local nonuniformity in electric field. In this study the interaction of a protoplast cell and electric field is investigated in detail. The effect of cell type on electric stress distribution on the cell surface under the application of non-uniform DC voltage is studied. The DEP force is calculated using both effective dipole approximation and Maxwell stress tensor and results are compared and difference of these two methods is discussed. The governing electrostatic equation is solved by immersed interface method (IIM) with considering particle shape.

2. Theory

A dielectric protoplast cell without ohmic loss with permittivity ε_p is considered to be immersed in a dielectric lossless fluid with permittivity ε_f. The cell is located at the center of a square enclosure with the length $a = 50$ μm. A DC voltage is applied on enclosure. The governing electrostatic equation is as Eq. 1. $\Phi(x,y)$ is electrostatic potential at point (x,y)

$$\nabla^2 \Phi = 0 \tag{1}$$

The boundary conditions are as follow:

$$\Phi(x,y) = \Phi_0 \quad \text{on electrode surfaces} \tag{2}$$

$$\frac{\partial \ddot{}(x,y)}{\partial n} = 0 \quad \text{on insulating surfaces}$$

The schematic of a protoplast cell and electric model of the problem is shown in Fig. 1.

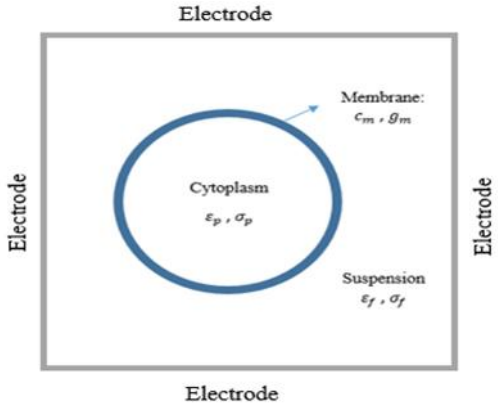

Fig. 1. A Schematic of the protoplast cell. Computational domain

The general internal boundary conditions (jump conditions) of a protoplast cell exposed to an electric field is as follow [17].

$$\underline{\pounds}_p \underline{E}_{r_p} = \underline{\pounds}_f \underline{E}_{r_f} \quad \text{at } r = R \tag{3-a}$$

$$\left(j\mu c_m + g_m\right)\left(\underline{\Phi}_1 - \underline{\Phi}_2\right) = -j\mu \underline{\pounds}_p \underline{E}_{r_p} \quad \text{at } r = R \tag{3-b}$$

Where $E_r = -\partial \ddot{} / \partial r$ and $\underline{\pounds} = \pounds_r - j\pounds_i = \pounds - j\pm/\mu$ is the complex permittivity. σ is ohmic conductivity and $\mu = 2\circledR f$ in which f is the frequency of applied electric field. Cell membrane is typically characterized by effective capacitance c_m and conductance g_m both per unit of surface area. In some practical cases in which applied voltage is DC or ohmic losses can be ignored, the boundary condition on interface can be simplified as Eq. 4:

$$\begin{aligned} &\ddot{}_p(x,y) = \ddot{}_f(x,y) \\ &\pounds_p \frac{\partial \ddot{}_p}{\partial \overline{n}} = \pounds_f \frac{\partial \ddot{}_f}{\partial \overline{n}} \end{aligned} \tag{4}$$

As mentioned, electric stresses acting on cell surface in the presence of electric field are calculated using Maxwell stress tensor. The surface integral of electric stress is the net DEP force applied on cell. Since electromagnetic effect is ignored, Maxwell stress tensor is expressed as Eq. 5. E_i and E_j are electric field vector components:

$$T_{ij} = \pounds\left(E_i E_j - \frac{1}{2}E^2 \copyright_{ij}\right) \tag{5}$$

Then surface DEP force density can be calculated by Eq. 6:

$$\overline{f} = \pounds\left(\overline{E}\cdot\overline{n}\right)\overline{E} - \frac{1}{2}\pounds E^2 \overline{n} \tag{6}$$

DEP force density must be calculated on both sides of interface. The net electric stress is the resultant of inner and outer stresses. Subscript 1 shows the cell side and number 2 shows the suspension side in the Eq. 7. As shown in Fig. 2, n is the normal vector of interface.

$$\overline{f}_1 = \pounds_p\left(\overline{E}_1\cdot\overline{n}_1\right)\overline{E}_1 - \frac{1}{2}\pounds_p {E_1}^2 \overline{n}_1 \tag{7-a}$$

$$\overline{f}_2 = \pounds_f\left(\overline{E}_2\cdot\overline{n}_2\right)\overline{E}_2 - \frac{1}{2}\pounds_f {E_2}^2 \overline{n}_2 \tag{7-b}$$

3. Solving method

With the aim of studying the electric stresses acting on cell in the presence of electric field, the electrostatic equation, which is the well-known Laplace equation 1 must be solved with considering the cell shape. So a proper solving method must be selected which can exactly implement the internal boundary conditions on the interface that make the problem well-posed. In this study, immersed interface method (IIM) is used to solve the governing equation. There are other approaches such as boundary element method. But the special feature of IIM is that it doesn't need to Green's function and it is applicable to general PDEs with or without source term. IIM is based on finite difference method or finite element method [31]. There are other modified finite difference methods such as smoothing method, harmonic averaging and well-known IBM to solve PDEs which their coefficient is discontinuous or there is singular force on interface [32,33]. These methods use smoothed Heaviside and discrete delta functions to implement the coefficient discontinuities.

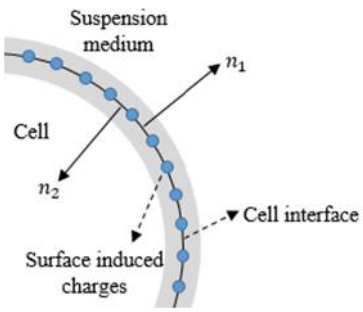

Fig. 2. Normal vectors of interface

IIM first introduced by Z. Li [33]. One obvious feature of IIM is using fixed and uniform mesh which has almost no cost for grid generation. Another characteristic of this approach is that the IIM uses the standard 5-point central finite difference scheme at all grid points and only adds a nonzero correction term to the right hand side of the finite difference equations at grid points near or on the interface. In this paper, fast IIM is used to discretize the equation. Fast IIM is a modified immersed interface method for solving equations which their coefficient is constant in both domains and it has a jump on interface. For more details about fast IIM refer to [33]. The main idea of fast IIM is weighted least square interpolation. For testing the solution algorithm, a 2D elliptic equation like Eq. 8 is solved by fast IIM and the numerical result is compared with exact solution.

$$\nabla\cdot\left(\quad(x,y)\nabla u\right)=f(x,y) \tag{8}$$

The interface in the domain $[-1,1]\times[-1,1]$ is expressed as Eq. 9.

$$\begin{cases} X=\left(r_0+0.2\sin\left(\mu^{-}\right)\right)\cos^{-}+x_c \\ Y=\left(r_0+0.2\sin\left(\mu^{-}\right)\right)\sin^{-}+y_c \end{cases} \qquad 0\le^{-}\le 2 \tag{9}$$

The exact solution is as Eq. 10 in which $\Omega^{\pm}$ is the domain inside/outside the interface.

$$u(x,y)=\begin{cases} \dfrac{r^2}{-} & if\ (x,y)\in\Omega^{-} \\ \left(\dfrac{r^4+C_0\log(2r)}{+}-\right. & \\ C_1\left(\dfrac{r_0^2}{-}-\right. & \\ \left.\left.\dfrac{r_0^4}{+}+\right.\right. & \\ \left.\left.\dfrac{C_0\log(2r_0)}{+}\right)\right) & if\ (x,y)\in\Omega^{+} \end{cases} \tag{10}$$

In which, $r=\sqrt{x^2+y^2}$. Dirichlet boundary equation and jump conditions are determined from exact solution. Consider the force as Eq. 11.

$$f(x,y)=\begin{cases} \dfrac{4}{-} & if\ (x,y)\in\Omega^{-} \\ \dfrac{16r^2}{+} & if\ (x,y)\in\Omega^{+} \end{cases} \tag{11}$$

The problem is solved using 5-point central difference stencil for $\mu=3$, $r_0=1/2$, $C_0=-0.1$, $C_1=1$, $^{-}=1$ and $^{+}=100$. In Fig. 3 the considered uniform mesh is shown. Regular and irregular grid points are shown by blue and red.

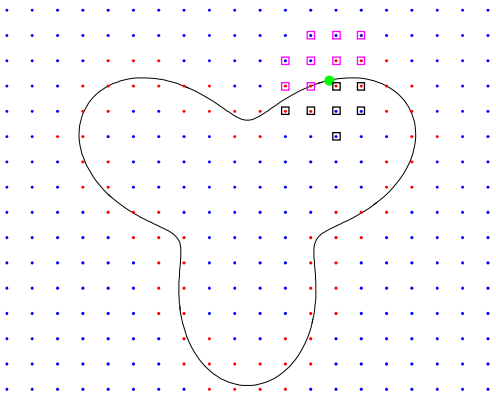

Fig. 3. The considered mesh. Blue and red points correspond to regular and irregular grid points respectively. The green point is the control point on interface at which surface derivative of φ is interpolated. The squares show points involved in interpolation.

Numerical solution is compared with the exact solution in figures 4 and 5. Fig. 4 shows the plots of exact and numeric solution. To closely compare the numeric and exact solution, solution is plotted at line $x=0$ and $y=0$ in Fig. 5. These figures show the good accuracy of solution algorithm. Figures 4 and 5 shows that fast IIM can satisfy the discontinuity in solution and its derivatives on the interface accurately.

The discrete form of Eq. 1 can be obtained using fast IIM (with 5-point central difference stencil) as presented in following equation, in which C_{ij} is the correction term which is zero at regular grid points [33]. In other words, the solution approach in regular grid points is the standard finite difference scheme. In the following equation Φ is the discrete form of ¨ and h is the mesh size.

$$\frac{1}{h^2}\left(\Phi_{i+1,j}+\Phi_{i-1,j}-4\Phi_{i,j}+\Phi_{i,j+1}+\Phi_{i,j-1}\right)=C_{ij} \tag{12}$$

Augmented variable is defined as Eq. 13 where ¦ is considered to be tangential direction on interface.

$$\frac{\partial^{¨}{}_{p}}{\partial\overline{n}}-\frac{\partial^{¨}{}_{f}}{\partial\overline{n}}=g\left(¦\right) \tag{13}$$

Discrete form of g is G. Interpolating surface derivatives of electrostatic potential on interface using

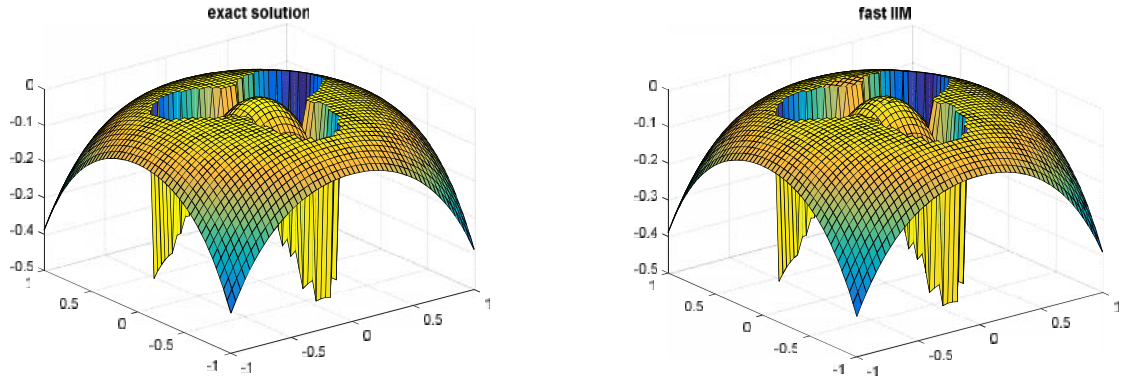

a **b**

Fig. 4. Plots of (a) exact solution and (b) numerical solution obtained by fast IIM with mesh size $h = 0.04$

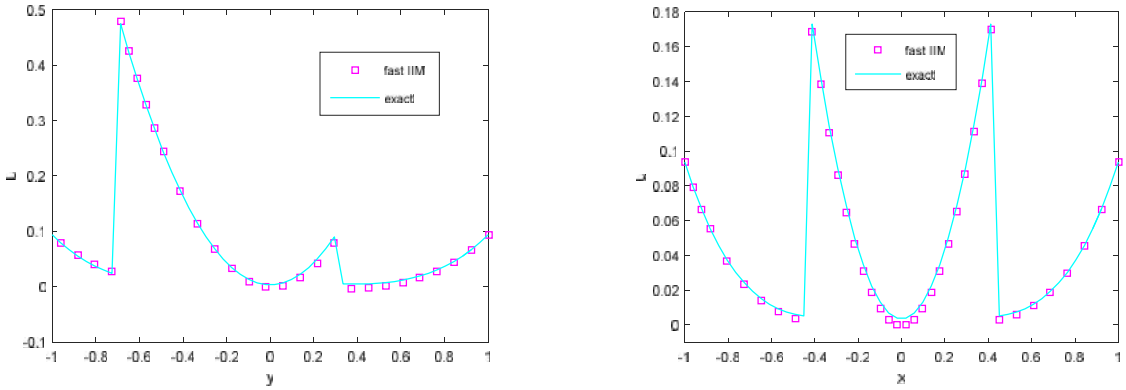

a **b**

Fig. 5. Comparing exact and numeric solutions at lines (a) $x = 0$ and (b) $y = 0$

weighted least square interpolation, the matrix form of Eq. 12 can be written as

$$\mathbf{A}\Phi + \mathbf{B}G = F_1 \tag{14}$$

Also the matrix form of Eq. 13 is obtained as Eq. 15:

$$\mathbf{E}\Phi + \mathbf{T}G = F_2 \tag{15}$$

It is not possible to express a closed form for matrices B, E, T, G, F_1 and F_2. They should be calculated element by element in a solution loop. Solving the following matrix equation, the problem can be solved:

$$\begin{bmatrix} \mathbf{A} & \mathbf{B} \\ \mathbf{T} & \mathbf{G} \end{bmatrix} \begin{bmatrix} \Phi \\ G \end{bmatrix} = \begin{bmatrix} F_1 \\ F_2 \end{bmatrix} \tag{16}$$

4. Results and discussion

When cell is exposed to electric field, it causes local changes in electrostatic potential and local nonuniformity in electric field. These changes in potential distribution are neglected in most previous works. In the present study the local nonuniformity caused by protoplast cell in an electric field is closely monitored and electric stresses acting on cell surface are investigated.

The first step in numerical analysis is convergence study. To examine the convergence of the solution, one can consider a cell with permittivity ratio $£_p/£_f = 10$ located at the center of a square enclosure with $a = 50$ μm. Vertical sides are insulated and a 1V DC voltage is applied to horizontal surfaces. The problem is solved for different mesh sizes. Fig. 6 shows the electrostatic potential at $x = 25$ μm. In this figure N is the number of control points on the interface. This figure shows that the mesh size $h = 0.8$ results in a good convergence.

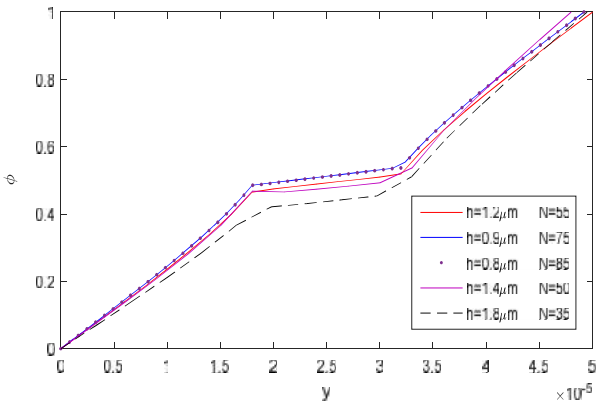

Fig. 6. Electrostatic potential (V) at $x = 25$ μm, $\varepsilon_p/\varepsilon_f = 10$

Now a protoplast cell with permittivity $£_p$ is considered immersed in a dielectric fluid with permittivity $£_f$. The cell is located at the center of a square enclosure under the application of non-uniform electric field. The potential boundary condition is as follow.

$$\begin{aligned} &¨ = 10^9 y^2 \quad \text{at } x = 0 \\ &¨ = 10^9 \left(y^2 - a^2\right) \quad \text{at } x = a \\ &¨ = 10^9 x^2 \quad \text{at } y = 0 \\ &¨ = 10^9 \left(a^2 - x^2\right) \quad \text{at } y = a \end{aligned} \tag{17}$$

The electrostatic potential distribution and electric field without considering the cell presence are shown in Fig. 7. Fig. 8 shows the effect of two kinds of protoplast cells (which their permittivity is lesser and more than the permittivity of surrounding fluid on electrostatic potential distribution). Fig. 9 shows local nonuniformity caused by the effect of two kinds of cells. The vectors show electric field vector in this picture. As can be seen in these figures, behavior of cell in electric field depends of its dielectric properties. So the electric stress distribution is expected to be different for these two kinds of cells. Since the applied voltage is DC, only the permittivity is important. But if the applied voltage is AC and ohmic loss of cell and suspension is not ignored, both conductivity and permittivity of cell and fluid must be considered [17]. Also the other important parameter which affects cell behavior is the Frequency of electric field.

As mentioned before, IIM is used to implement the internal boundary conditions on cell interface. In order to examine the accuracy of solution, electric filed is interpolated on interface and E_r which is $-\partial¨/\partial r$ has been calculated on both sides of the interface. Fig. 10 shows that jump condition is satisfied very good and it shows the good accuracy of solving algorithm.

In Fig. 11 electrostatic potential and electric field intensity at $x = 25\,\mu\text{m}$ are plotted. Cells with permittivity ratio $£_p/£_f = 0.02$ and $£_p/£_f = 10$ located at the center of the enclosure. In this figure red curves show the electrostatic potential and electric field intensity without considering the presence of the cell. Blue curves show the effect of cell in potential distribution and electric field. As can be seen in this figure, electric potential is continuous across the interface, but its gradient which is electric field is non-continuous. It can be observed that IIM has satisfied

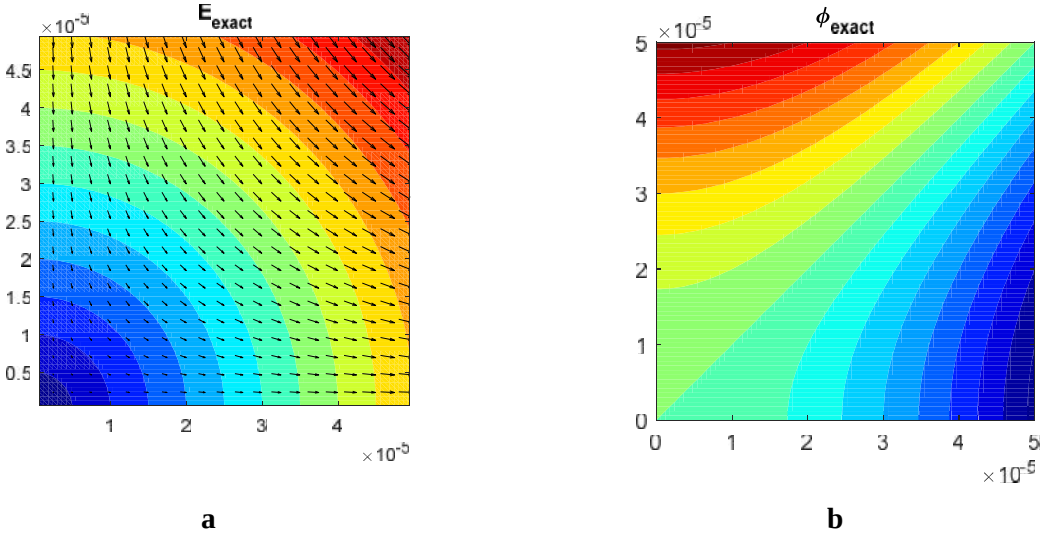

a **b**

Fig. 7. (a) Electric field and (b) electrostatic potential distribution without the effect of cell

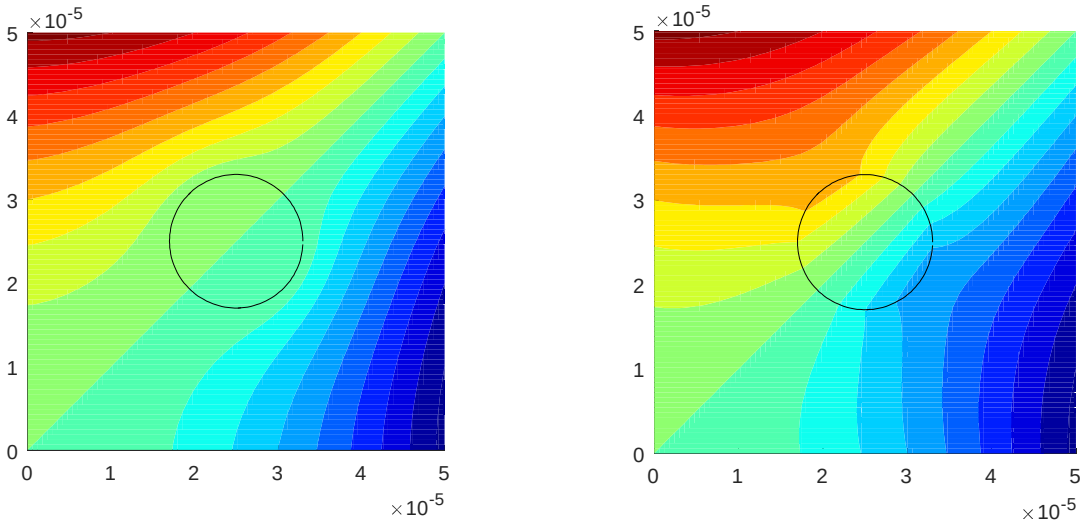

a b

Fig. 8. Local changes in electrostatic potential caused by protoplast cell with $R = 8$ μm, permittivity ratio (a) $\varepsilon_p/\varepsilon_f = 10$, and (b) $\varepsilon_p/\varepsilon_f = 0.02$

the discontinuity of solution accurately. Fig. 12 shows the interpolated electric field vectors on both sides of interface. Red and blue vectors indicate electric field vectors on suspension side and cell side respectively. The discontinuity of electric field is obvious in this picture.

Now we calculate DEP force using both MST and EDM method. Behavior of cell under the application of electric field as mentioned, depends on dielectric properties of cell and buffer and the frequency of applied voltage as well. Complex Clausius-Mossotti factor $\underline{K}(\mu)$ which is a function of dielectric properties of cell and fluid, determines the behavior of cell in electric field. DEP force depends upon the magnitude and sign of Clausius-Mossotti factor. Consistent to this, we choose to distinguish between pDEP and nDEP effects. If $\mathrm{Re}\left[\underline{K}(\mu)\right] > 0$ the cell is attracted toward higher electric field region. This phenomenon is called positive dielectrophoresis. If

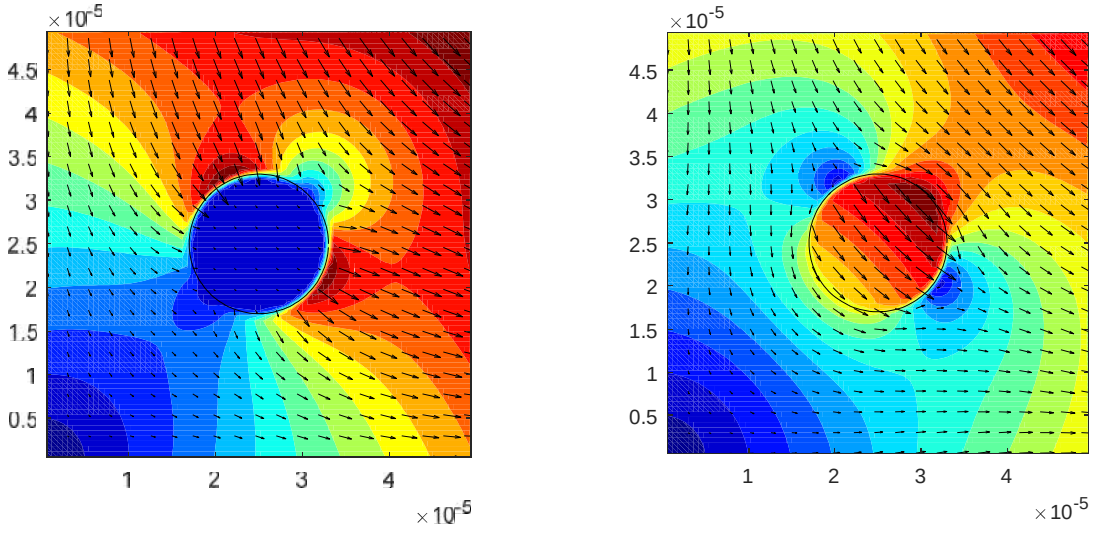

a **b**

Fig. 9. Local nonuniformity in electric field caused by protoplast cell with $R = 8$ μm, permittivity ratio (a) $\varepsilon_p/\varepsilon_f = 10$ and (b) $\varepsilon_p/\varepsilon_f = 0.02$

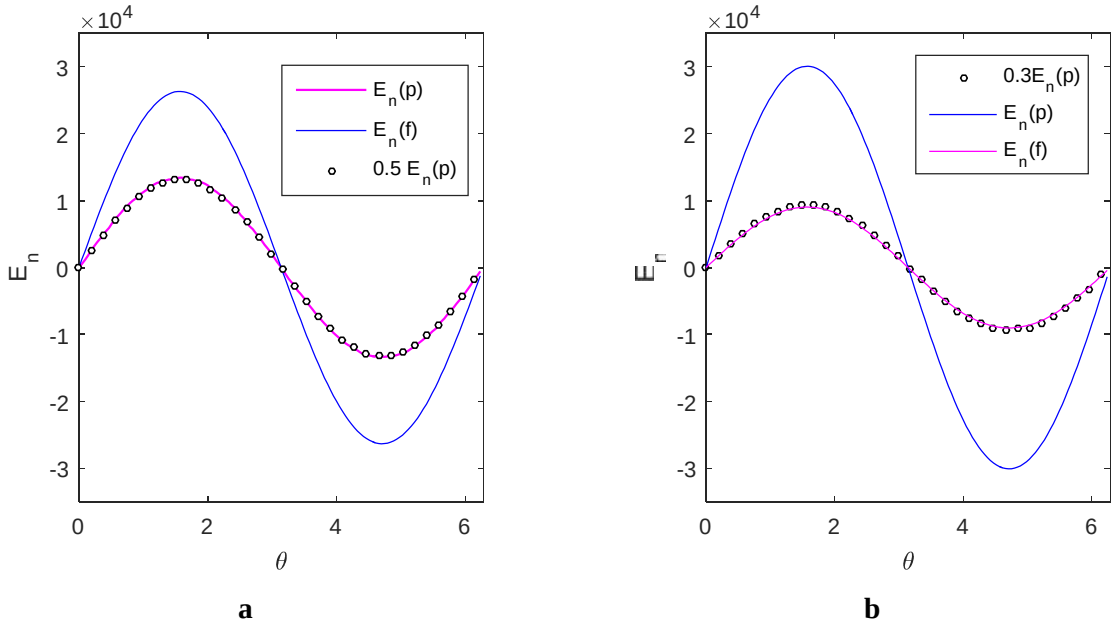

Fig. 10. Interpolated E_r on both sides of the interface of a cell with permittivity ratio (a) $\varepsilon_p/\varepsilon_f = 0.5$ and (b) $\varepsilon_p/\varepsilon_f = 0.3$

$\mathrm{Re}\left[\underline{K}(\mu)\right] < 0$ the cell is driven toward lower electric field region. It is called negative dielectrophoresis. If we ignore the ohmic loss of cell or the applied voltage is DC, the permittivity ratio $£_p/£_f$ distinguishes between pDEP and nDEP. If it is less or more than 1 cell experience nDEP and pDEP effects respectively.

DEP force using EDM approximation is calculated by Eq. 18.

$$\bar{F}_{DEP} = 2\pi £_f R^3 \left(\frac{£_p - £_f}{£_p + 2£_f}\right)\nabla E_0^2 \qquad (18)$$

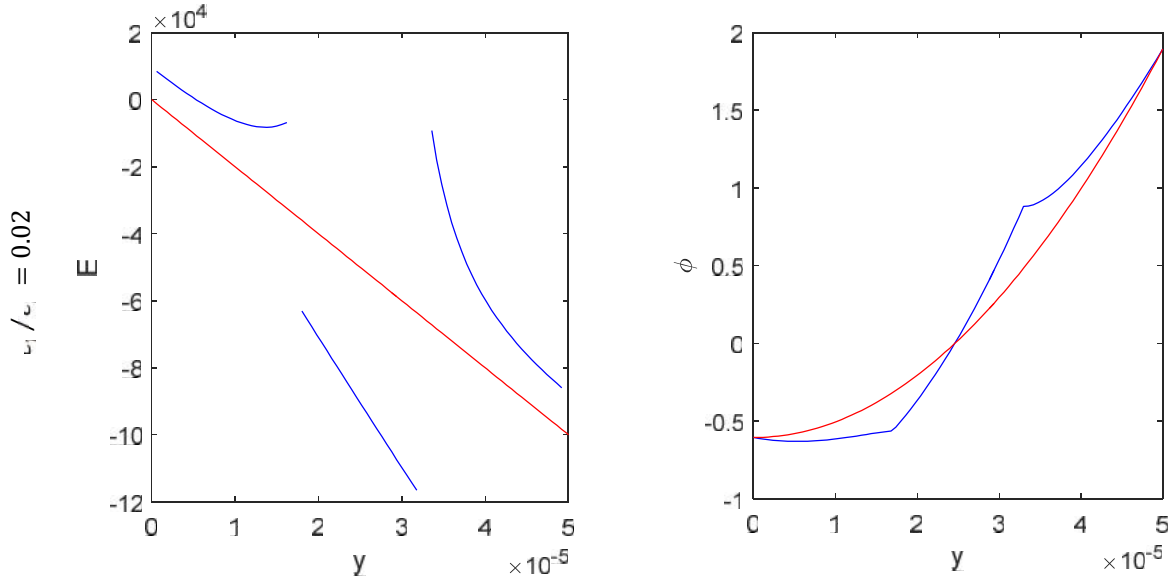

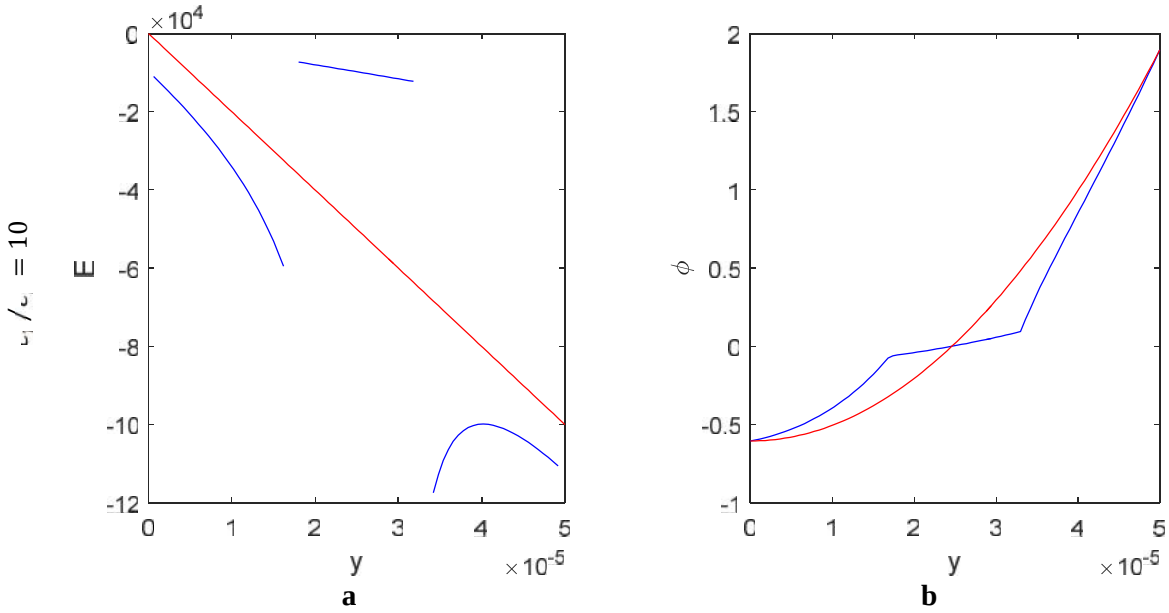

Fig. 11. (a) electric field intensity and (b) electrostatic potential (V) at $x = 25$ μm. Red curve shows the potential and electric field while cell does not present and blue curves show the effect of cell

In Fig. 13 nDEP and pDEP effects are shown. DEP force contour that is obtained from exact solution is plotted in this figure. In Fig. 13-a which shows nDEP $£_p = 2£_0$ and $£_f = 100£_0$. In Fig. 13-b in which pDEP effect is shown $£_p = 20£_0$ and $£_f = 2£_0$. Vectors show DEP force in this figure.

Electric field discontinuity on cell surface causes electric stresses on cell surface. DEP force can be calculated by integrating surface electric stresses. If the applied electric field is uniform, the net force is zero. In Fig. 14 electric stresses on cell surface with permittivity ratio $£_p/£_f = 0.02$ and $£_p/£_f = 10$ are shown. Red and blue vectors show electric force on suspension side and cell side respectively. Total electric stress distribution acting on cell membrane is shown in Fig. 15. As can be seen stress distribution is different for two different cell types.

As mentioned before, effective dipole moment (EDM) approximation is accurate only when the cell size is much smaller than the device size and its shape is simple. Now DEP force calculated using exact solution of electrostatic potential field will be compared with DEP force obtained by integrating the surface electric stresses. The results are presented in

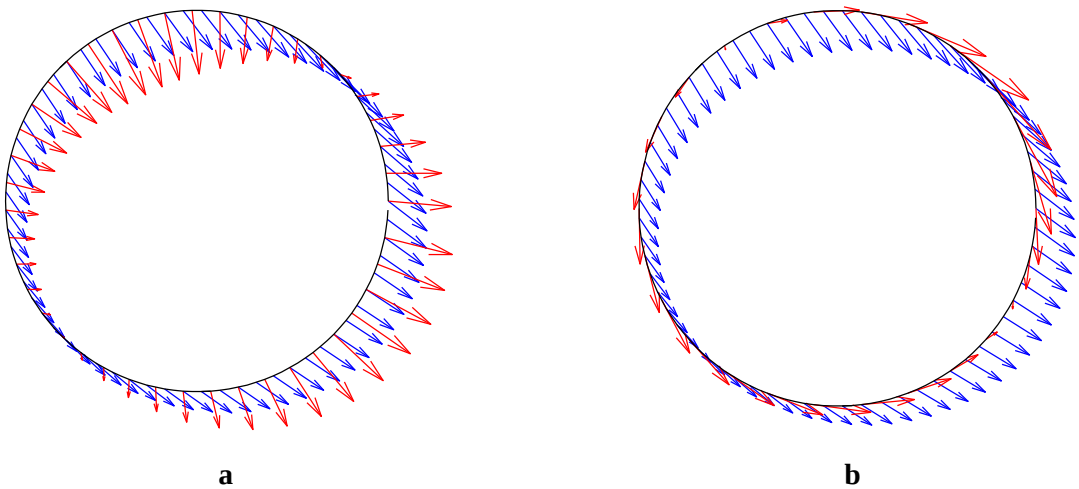

Fig. 12. Electric field vectors on cell surface. cell permittivity ratio is (a) $\varepsilon_p/\varepsilon_f = 10$ and (b) $\varepsilon_p/\varepsilon_f = 0.02$. Red and blue vectors indicate electric field vectors on suspension side and cell side respectively

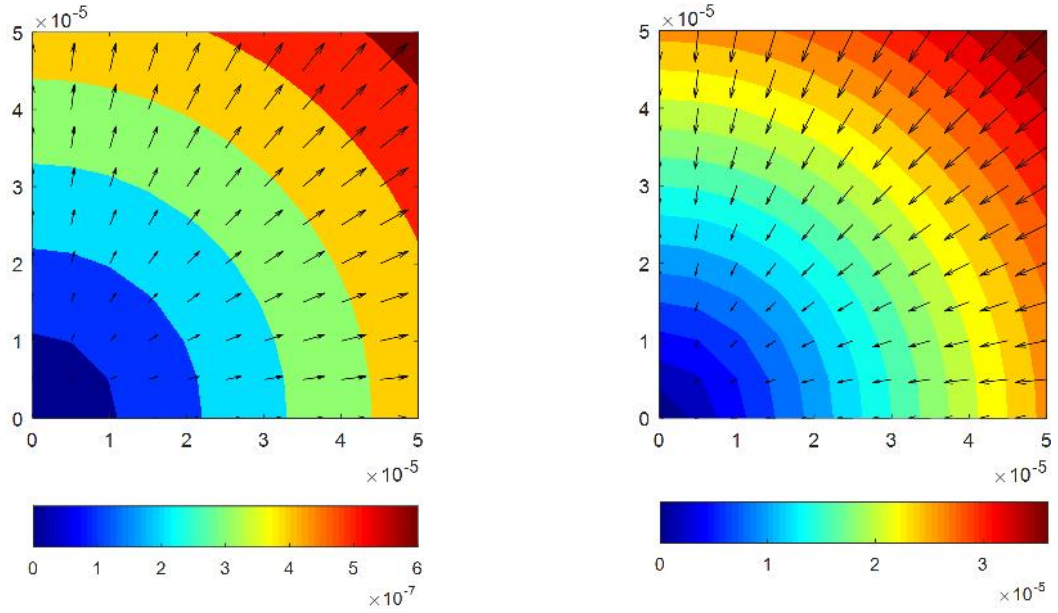

Fig. 13. DEP force (N) contours for (a) $\varepsilon_p = 2\varepsilon_0$, $\varepsilon_f = 100\varepsilon_0$ and (b) $\varepsilon_p = 20\varepsilon_0$, $\varepsilon_f = 2\varepsilon_0$. pDEP and nDEP effect are shown in (a) and (b) respectively

tables 1 to 4. The particle is located at $C_x = 25$ µm and $C_y = 25$ µm. As can be seen, when the cell radius is smaller than 3 µm the deviation of two methods is negligible. This shows that the solution algorithm is valid. But when the cell radius increases the accuracy of EDM approximation decreases. Results for cell with permittivity ratio $£_p/£_f < 1$ and $£_p/£_f > 1$ are presented in tables 1 and 2 and tables 3 and 4 respectively.

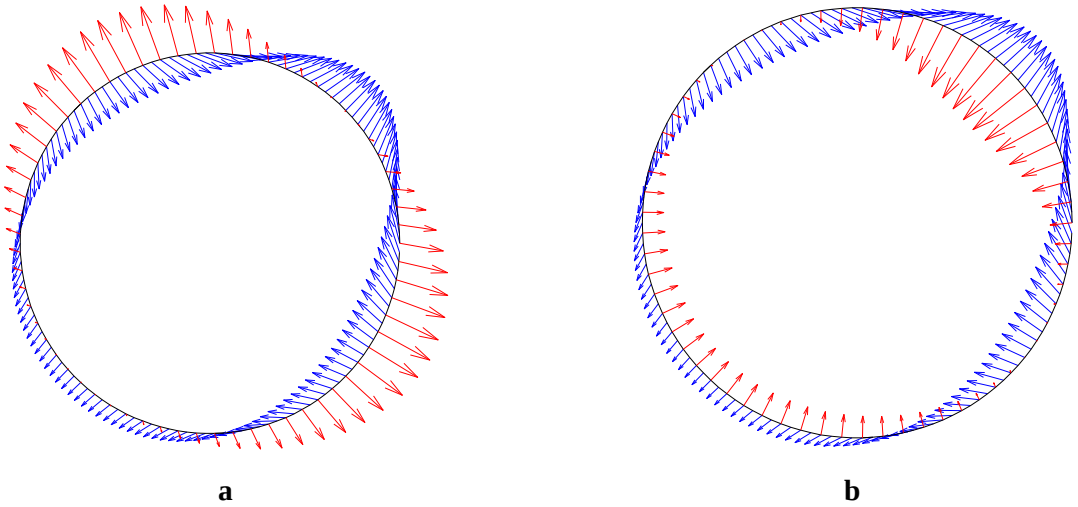

Fig. 14. DEP force density on both sides of interface of protoplast cell under the application of non-uniform electric field. Cell radius is 8 µm. (a) $\varepsilon_p = 20\varepsilon_0$, $\varepsilon_f = 2\varepsilon_0$ and (b) $\varepsilon_p = 2\varepsilon_0$, $\varepsilon_f = 100\varepsilon_0$. Red and blue vectors show the DEP force density on suspension and cell side respectively

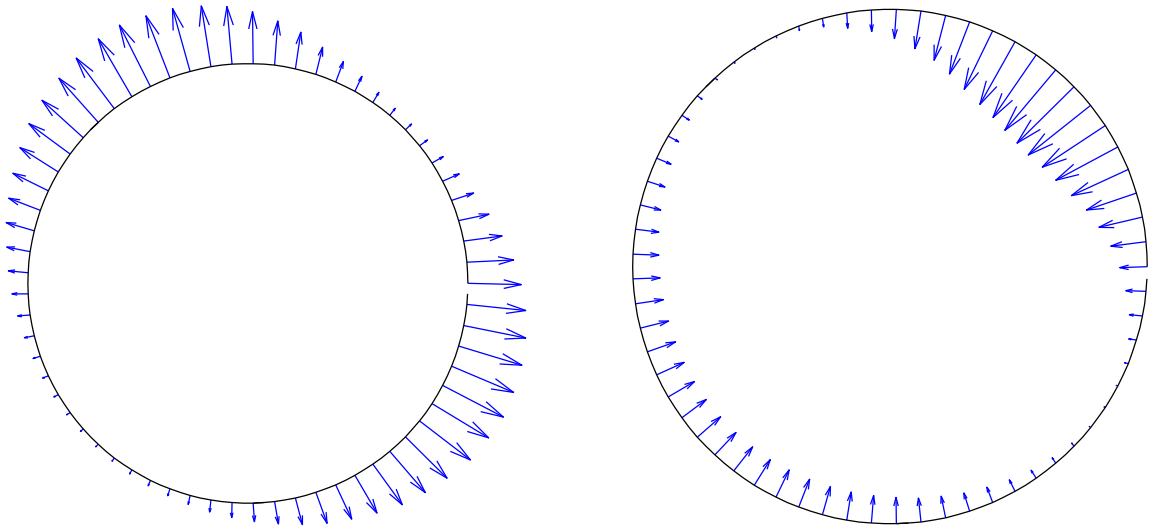

a **b**

Fig. 15. Electric stress distribution on the cell surface with radius 8 μm. (a) $\varepsilon_p = 20\varepsilon_0$, $\varepsilon_f = 2\varepsilon_0$ and (b) $\varepsilon_p = 2\varepsilon_0$, $\varepsilon_f = 100\varepsilon_0$.

Table 1. comparing MST and EDM methods. $\varepsilon_p/\varepsilon_f = 0.02$

R (μm)	F_{EDM} (N)	F_{MST} (N)	error (%)
2	3.02×10^{-6}	3×10^{-6}	0.666
3	6.8×10^{-6}	7.05×10^{-6}	3.546
4	1.21×10^{-5}	1.12×10^{-5}	8.035
5	1.89×10^{-5}	1.71×10^{-5}	10.52
6	2.72×10^{-5}	2.46×10^{-5}	10.56
7	3.7×10^{-5}	3.32×10^{-5}	11.44
8	4.84×10^{-5}	4.24×10^{-5}	14.15
9	6.12×10^{-5}	5.21×10^{-5}	17.46
10	7.56×10^{-5}	6.38×10^{-5}	18.49

Table 2. comparing MST and EDM methods. $\varepsilon_p/\varepsilon_f = 0.2$

R (μm)	F_{EDM} (N)	F_{MST} (N)	error (%)
2	1.05×10^{-6}	1.04×10^{-6}	0.96
3	2.36×10^{-6}	2.3×10^{-6}	2.60
4	4.19×10^{-6}	3.92×10^{-6}	6.88
5	6.55×10^{-6}	6.08×10^{-6}	7.73
6	9.44×10^{-6}	8.71×10^{-6}	8.38
7	1.28×10^{-5}	1.18×10^{-5}	8.47
8	1.68×10^{-5}	1.51×10^{-5}	11.25
9	2.12×10^{-5}	1.87×10^{-5}	13.36
10	2.62×10^{-5}	2.28×10^{-5}	14.91

Table 3. comparing MST and EDM methods. $\varepsilon_p/\varepsilon_f = 10$

R (μm)	F_{EDM} (N)	F_{MST} (N)	error (%)
3	2.89×10^{-7}	2.91×10^{-7}	0.48
4	5.15×10^{-7}	5.18×10^{-7}	0.68
5	8.04×10^{-6}	8.12×10^{-6}	0.87
6	1.16×10^{-6}	1.17×10^{-6}	1.09
7	1.57×10^{-6}	1.63×10^{-6}	3.60
8	2.06×10^{-6}	2.19×10^{-6}	6.16
9	2.60×10^{-6}	2.86×10^{-6}	10.05
10	3.21×10^{-6}	3.66×10^{-6}	14.10

Table 4. comparing MST and EDM methods. $\varepsilon_p/\varepsilon_f = 50$

R (μm)	F_{EDM} (N)	F_{MST} (N)	error (%)
3	1.36×10^{-7}	1.36×10^{-7}	0.12
4	2.42×10^{-7}	2.55×10^{-7}	0.55
5	3.77×10^{-7}	3.86×10^{-7}	2.43
6	5.44×10^{-7}	5.58×10^{-7}	2.46
7	7.41×10^{-7}	7.73×10^{-7}	4.38
8	9.67×10^{-6}	1.05×10^{-6}	8.33
9	1.22×10^{-6}	1.37×10^{-6}	12.14
10	1.51×10^{-6}	1.77×10^{-6}	16.82

5. Conclusion

Cells are exposed to external electric fields in many biomedical and biological applications such as electroporation and electrofusion. Therefore, it is necessary to closely study the interaction of cells and electric field. The most famous effect of electric field on cells is the dielectrophoresis phenomenon. In the previous researches mostly the behavior of a cell group under the application of electric field has been studied due to design microfluidics systems for medical applications like particle separating, assembly and filtration. But in this study the behavior of a single cell in the presence of non-uniform electric field is studied. To this end, we needed to solve the governing equations with considering the cell presence in the solution domain. IIM is used to solve the governing equations. Some numerical results are presented to examine the accuracy of IIM to satisfy the internal boundary conditions on the cell interface. By calculating Maxwell stress tensor, electric stress distribution on cell surface is investigated. In order to examine the validity of solution and the accuracy of EDM, we compared DEP force calculated using EDM method and DEP force obtained by integrating Maxwell stress tensor. Results are matched when the cell radius is smaller than 3 μm. It shows that solution method is valid. But when cell radius is more than 3 μm EDM approximation becomes very inaccurate. The results of this research can help to better understanding the phenomenon electroporation.

6. References

[1] H. A. Pohl, Some effects of nonuniform fields on dielectrics, *Journal of Applied Physics*, Vol. 29, No. 8, pp. 1182-1188, 1958.

[2] X. Feng, W. Du, Q. Luo, B.-F. Liu, Microfluidic chip: next-generation platform for systems biology, *Analytica Chimica Acta*, Vol. 650, No. 1, pp. 83-97, 2009.

[3] K. Khoshmanesh, N. Kiss, S. Nahavandi, C. W. Evans, J. M. Cooper, D. E. Williams, D. Wlodkowic, Trapping and imaging of micron-sized embryos using dielectrophoresis, *Electrophoresis*, Vol. 32, No. 22, pp. 3129-3132, 2011.

[4] J. P. Vacanti, R. Langer, Tissue engineering: the design and fabrication of living replacement devices for surgical reconstruction and transplantation, *The Lancet*, Vol. 354, pp. S32-S34, 1999.

[5] B. H. Weigl, R. L. Bardell, C. R. Cabrera, Lab-on-a-chip for drug development, *Advanced drug delivery reviews*, Vol. 55, No. 3, pp. 349-377, 2003.

[6] P. C. Li, D. J. Harrison, Transport, manipulation, and reaction of biological cells on-chip using electrokinetic effects, *Analytical Chemistry*, Vol. 69, No. 8, pp. 1564-1568, 1997.

[7] E. Verpoorte, Microfluidic chips for clinical and forensic analysis, *Electrophoresis*, Vol. 23, No. 5, pp. 677-712, 2002.

[8] Y. Cho, S. Lee, B. Kim, T. Fujii, Fabrication of silicon dioxide submicron channels without

nanolithography for single biomolecule detection, *Nanotechnology*, Vol. 18, No. 46, pp. 465303, 2007.

[9] S. K. Sia, G. M. Whitesides, Microfluidic devices fabricated in poly (dimethylsiloxane) for biological studies, *Electrophoresis*, Vol. 24, No. 21, pp. 3563-3576, 2003.

[10] R. Pethig, G. H. Markx, Applications of dielectrophoresis in biotechnology, *Trends in biotechnology*, Vol. 15, No. 10, pp. 426-432, 1997.

[11] L. Zheng, J. P. Brody, P. J. Burke, Electronic manipulation of DNA, proteins, and nanoparticles for potential circuit assembly, *Biosensors and Bioelectronics*, Vol. 20, No. 3, pp. 606-619, 2004.

[12] P. R. Gascoyne, J. Vykoukal, Particle separation by dielectrophoresis, *Electrophoresis*, Vol. 23, No. 13, pp. 1973, 2002.

[13] R. Pethig, Review article—dielectrophoresis: status of the theory, technology, and applications, *Biomicrofluidics*, Vol. 4, No. 2, pp. 022811, 2010.

[14] X. Wang, X.-B. Wang, P. R. Gascoyne, General expressions for dielectrophoretic force and electrorotational torque derived using the Maxwell stress tensor method, *Journal of electrostatics*, Vol. 39, No. 4, pp. 277-295, 1997.

[15] T. Jones, M. Washizu, Multipolar dielectrophoretic and electrorotation theory, *Journal of Electrostatics*, Vol. 37, No. 1, pp. 121-134, 1996.

[16] C. H. Kua, Y. C. Lam, C. Yang, K. Youcef-Toumi, I. Rodriguez, Modeling of dielectrophoretic force for moving dielectrophoresis electrodes, *Journal of Electrostatics*, Vol. 66, No. 9, pp. 514-525, 2008.

[17] T. Jones, Electromechanics of ParticlesCambridge Univ, *Press, Cambridge*, 1995.

[18] N. G. Green, T. B. Jones, Numerical determination of the effective moments of non-spherical particles, *Journal of Physics D: Applied Physics*, Vol. 40, No. 1, pp. 78, 2006.

[19] A. Ogbi, L. Nicolas, R. Perrussel, S. J. Salon, D. Voyer, Numerical identification of effective multipole moments of polarizable particles, *IEEE Transactions on Magnetics*, Vol. 48, No. 2, pp. pp 675-678, 2012.

[20] D. L. House, H. Luo, Effect of direct current dielectrophoresis on the trajectory of a non-conducting colloidal sphere in a bent pore, *Electrophoresis*, Vol. 32, No. 22, pp. 3277-3285, 2011.

[21] Y. Liu, W. K. Liu, T. Belytschko, N. Patankar, A. C. To, A. Kopacz, J. H. Chung, Immersed electrokinetic finite element method, *International Journal for Numerical Methods in Engineering*, Vol. 71, No. 4, pp. 379-405, 2007.

[22] R. Saunders, Static magnetic fields: animal studies, *Progress in biophysics and molecular biology*, Vol. 87, No. 2, pp. 225-239, 2005.

[23] A. Pazur, C. Schimek, P. Galland, Magnetoreception in microorganisms and fungi, *Open Life Sciences*, Vol. 2, No. 4, pp. 597-659, 2007.

[24] R. H. W. Funk, T. Monsees, N. Özkucur, Electromagnetic effects–From cell biology to medicine, *Progress in histochemistry and cytochemistry*, Vol. 43, No. 4, pp. 177-264, 2009.

[25] J. Miyakoshi, Effects of static magnetic fields at the cellular level, *Progress in biophysics and molecular biology*, Vol. 87, No. 2, pp. 213-223, 2005.

[26] T. Sakurai, S. Terashima, J. Miyakoshi, Effects of strong static magnetic fields used in magnetic resonance imaging on insulin-secreting cells, *Bioelectromagnetics*, Vol. 30, No. 1, pp. 1-8, 2009.

[27] S. Di, Z. Tian, A. Qian, J. Li, J. Wu, Z. Wang, D. Zhang, D. Yin, M. L. Brandi, P. Shang, Large gradient high magnetic field affects FLG29. 1 cells differentiation to form osteoclast-like cells, *International journal of radiation biology*, Vol. 88, No. 11, pp. 806-813, 2012.

[28] V. Zablotskii, T. Polyakova, O. Lunov, A. Dejneka, How a High-Gradient Magnetic Field Could Affect Cell Life, *Scientific Reports*, Vol. 6, 2016.

[29] L. D'Amico, N. J. Ajami, J. A. Adachi, P. R. C. Gascoyne, J. F. Petrosino, Isolation and concentration of bacteria from blood using microfluidic membraneless dialysis and dielectrophoresis, *Lab on a Chip*, Vol. 17, No. 7, pp. 1340-1348, 2017.

[30] M. Antfolk, S. H. Kim, K. Saori, S. Kaneda, T. Fujii, T. Laurell, An integrated acousto-and dielectrophoresis device for tumor cell separation, concentration, and single-cell trapping, in *Proceeding of*, Chemical and Biological Microsystems Society, pp. 1657-1658.

[31] Z. Li, The immersed interface method using a finite element formulation, *Applied Numerical Mathematics*, Vol. 27, No. 3, pp. 253-267, 1998.

[32] Z. Li, K. Ito, 2006, *The immersed interface method: numerical solutions of PDEs involving interfaces and irregular domains*, Siam,

[33] R. J. Leveque, Z. Li, The immersed interface method for elliptic equations with discontinuous coefficients and singular sources, *SIAM Journal on Numerical Analysis*, Vol. 31, No. 4, pp. 1019-1044, 1994.

[34] M. R. Hossan, R. Dillon, A. K. Roy, P. Dutta, Modeling and simulation of dielectrophoretic particle–particle interactions and assembly, *Journal of colloid and interface science*, Vol. 394, pp. 619-629, 2013.

[35] I. Isaac Hosseini, and M. Moghimi Zand, Optimized Microstructure for Single Cell Trapping Utilizing Contactless Dielectrophoresis, *Journal of Thermal Engineering*, in press.

[36] M. Shiri, M. Moghimi Zand, Design and simulation of a novel motile sperm separation microfluidic system by use of electrophoresis, *Sharif Journal*, in press.